Journal of Alloys and Compounds 509 (2011) 9901–9905

Contents lists available at ScienceDirect

Journal of Alloys and Compounds

journal homepage: www.elsevier.com/locate/jallcom

Preparation, characterization and the electrogenerated chemiluminescence behavior of WO_3 nanocrystals

Qihua Huang[a], Lishi Wang[a,*], Min Wang[a], Junmin Nan[b,*]

[a] School of Chemistry and Chemical Engineering and State Key Laboratory of Pulp and Paper Engineering, South China University of Technology, Guangzhou 510640, China
[b] School of Chemistry and Environment, South China Normal University, Guangzhou 510006, China

ARTICLE INFO

Article history:
Received 6 April 2011
Received in revised form 21 July 2011
Accepted 22 July 2011
Available online 29 July 2011

Keywords:
Nanostructured materials
Oxide materials
Optical properties
Luminescence

ABSTRACT

The $(WO_3)_{NCs}$/Nafion film electrode was prepared by immobilizing the synthesized WO_3 NCs on the surface of a glassy carbon electrode (GCE) with the help of Nafion. The ECL emission of the electrode in aqueous solution was affected by the buffer solution with respect to the pH and composition. And the strongest ECL was observed in an NH_3–NH_4Cl buffer with pH being 8.2. Only a weak ECL peak at 1.14 V which was originated from the annihilation process between oxidized and reduced species of WO_3 NCs was found. By adding coreactant triproplamine (TPrA) in buffer solution, an additional ECL peak at 1.13 V which was attributed to the electron-transfer reaction between the oxidized WO_3 NCs and reduced intermediate of TPrA was observed. The $(WO_3)_{NCs}$/Nafion film electrode exhibits excellent ECL property and good stability, which would promote the potential application of WO_3 NCs as a luminescence material for solid-state ECL detection.

© 2011 Elsevier B.V. All rights reserved.

1. Introduction

Electrogenerated chemiluminescence (ECL) is originated from the electron-transfer reaction of an excited redox species on the electrode surface. Owing to its inherent features, such as low detection limit, simplified optical setup and very low background signal, ECL has become an important and valuable detection method in analytical chemistry over the past several decades [1]. Among the popular ECL reagents like Luminol, lucigenin, aryl oxalates, acridinium esters, dioxetanes and $Ru(bpy)_3^{2+}$[2], $Ru(bpy)_3^{2+}$ has been extensively studied and exploited because of its excellent characteristics of strong luminescence and high solubility in aqueous and nonaqueous solvents, good chemical stability and high ECL efficiency, and employed as the labels of biological molecules in immunoassays and DNA analyses [3,4]. As $Ru(bpy)_3^{2+}$ is regenerated during the ECL process, solid-state ECL sensors can be fabricated by immobilizing $Ru(bpy)_3^{2+}$ on an electrode surface. Compared with solution-state ECL system, solid-state ECL can reduce the consumption of expensive ECL reagent $Ru(bpy)_3^{2+}$, enhance the ECL signal and simplify experimental design [5]. However, $Ru(bpy)_3^{2+}$ ECL sensors has some limitations, for example, $Ru(bpy)_3^{2+}$ labeling at multiple sites of the biomolecule may result in the loss of biological activity of targets [6].

The ECL behavior of semiconductor NCs, including compound semiconductor NCs such as CdSe and CdTe and elemental semiconductor NCs such as Si and Ge, has attracted tremendous attention because semiconductor NCs can be electrically excited in both aqueous and nonaqueous media [7–11]. While the low solubility and instability of the redox species of semiconductor NCs in solution phase limit the development of semiconductor NCs sensors on the basis of ECL of semiconductor NCs [7,9], the thin-film technique of semiconductor NCs provide an effective alternative way for constructing novel ECL sensors owing to the excellent stability and high ECL intensity of semiconductor NCs thin film [12].

The transition metal-oxide semiconductor NCs have been demonstrated their potential application in solar cells, catalysts, and etc. [13–18]. Among the numerous transition metal-oxide semiconductors, tungsten trioxide (WO_3) has outstanding electrochromic, gaschromic, thermochromic and optochromic properties, and has been widely used in smart windows [19], electrochemical sensors [20], semiconductor gas sensors [21], photodetectors [22], electrocatalysts [23] and photocatalysts [24] in recent years. In addition, considerable efforts have been made to investigate the coloration efficiency [25], photon–electron conversion efficiency [26], photoelectrochemical properties [27] and photoluminescence (PL) behavior [28] of WO_3. However, it is noted that the ECL behavior of WO_3 has rarely been reported. Given that the cost of WO_3 is lower than that of $Ru(bpy)_3^{2+}$, it is meaningful to study the ECL behavior of WO_3. In this paper, the WO_3 NCs were prepared by a facile hydrothermal method and characterized by XRD, XPS, SEM, PL and UV–vis spectra. The as-synthesized WO_3 NCs

* Corresponding authors. Tel.: +86 20 87112906; fax: +86 20 87112906.
E-mail addresses: wanglsh@scut.edu.cn (L. Wang), jmnan@scnu.edu.cn (J. Nan).

0925-8388/$ – see front matter © 2011 Elsevier B.V. All rights reserved.
doi:10.1016/j.jallcom.2011.07.082

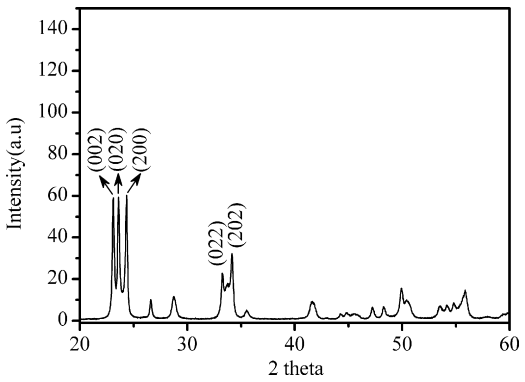

Fig. 1. X-ray diffraction patterns of WO_3 NCs.

were further immobilized on the surface of a glassy carbon electrode (GCE) with the help of Nafion to obtain the $(WO_3)_{NCs}$/Nafion film electrode. The ECL behavior of $(WO_3)_{NCs}$/Nafion film electrode in aqueous solution with and without the presence of coreactant tripropylamine (TPrA) was investigated and the possible ECL mechanism was proposed.

2. Experimental

Ammonium tungstate hydrate ($H_{40}N_{10}O_{41}W_{12}{\cdot}xH_2O$) and cetyltrimethylammonium bromide ($C_{19}H_{49}BrN$) were purchased from Sinopharm Chemical Reagent Co. Ltd. and Shanghai Bio Life Science and Technology Co. Ltd., respectively. The 5 wt% Nafion (purchased from Sigma) was diluted with ethanol to 0.05 wt%. All chemicals were of analytical grade and used without further purification. Twice-distilled water was used throughout all experiments. High-purity nitrogen was used for air-free condition.

The WO_3 NCs were synthesized by a hydrothermal reaction and post calcinations according to the literature procedure [29]. In a typical synthesis, 1.478 g $H_{40}N_{10}O_{41}W_{12}{\cdot}xH_2O$ and 6.56 g $C_{19}H_{49}BrN$ were suspended in 50 mL of water and pH was adjusted to 8–9 using $NH_3{\cdot}H_2O$ solution with stirring. After achieving complete dissolution of the precursor, the solution was transferred to five Teflon-lined autoclaves with 10 mL of internal volume and kept in an oven for 24 h at 140 °C. The precipitate was collected through centrifugation and thoroughly washed with water, and then dried at 100 °C followed by calcinations in air atmosphere at 600 °C for 10 h. The as-synthesized WO_3 NCs were dispersed in water under ultrasonication for 30 min to obtain the 0.5 mg mL^{-1} WO_3 suspension. The bare GCE with 2 mm in diameter was polished with α-alumina powders and rinsed with ethanol, acetone and water orderly. 3.0 μL of 0.5 mg mL^{-1} WO_3 suspension ($\sim 3.8 \times 10^{-8}$ mol) was dropped onto the surface of GCE and dried at room temperature, and then 1.0 μL of 0.05% Nafion was coated on the WO_3 modified electrode. The $(WO_3)_{NCs}$/Nafion film electrode was finally prepared after evaporating the solvent at room temperature.

The phase composition of the as-prepared WO_3 NCs was identified by X-ray diffractometer (XRD, Bruker, Germany) at 40 kV, 40 mA with an Cu Kα radiation (λ = 0.154 nm). X-ray photoelectron spectroscopy (XPS) measurements were performed with Axis Ultra^{DLD} (Kratos, Japan). Scanning electron microscopy (SEM) analysis was conducted using a LEO-1530VP (Hitachi, Japan). The UV–vis absorbance and PL spectrum were checked by using a UV 3010 (Hitachi, Japan) and F-4500 spectrophotometer (Hitachi, Japan). ECL signals were recorded with a homemade ECL system containing a three-electrode system consisted of a $(WO_3)_{NCs}$/Nafion film electrode, a platinum counter electrode, and a saturated calomel reference electrode. During the measurement, the potential was applied to the working electrode via a CHI660B electrochemical workstation (Shanghai Chenhua, China) and the ECL emission was detected with a photomultiplier tube (PMT) biased at −850 V.

3. Results and discussion

3.1. Characterization of WO_3 NCs

The XRD pattern of the as-synthesized WO_3 NCs is shown in Fig. 1. The sharp diffraction peaks appearing at 23.11°, 23.59°, 24.35°, 33.25°, 34.16° could be indexed to (002), (020), (200), (022) and (202) crystal planes, respectively. The peak location and intensity are in agreement with the standard diffraction data of monoclinic WO_3 form (JCPDS No.43–1035) [29], showing that the WO_3 NCs have monoclinic phase structure with high surface activity. The mean crystallite size (D) could be estimated from the full width at half-maximum (FWHM) of the diffraction peaks, using the Scherrer formula as follows:

$$D = \frac{K\lambda}{\beta \cos\theta} \quad (1)$$

where λ is the X-ray wavelength, θ is the diffraction angle, β is the FWHM, and $K = 0.89$ is a constant. The mean crystallite size of WO_3 NCs was estimated to be about 25 nm according to this formula.

In order to understand the components of the prepared WO_3 NCs, XPS was performed to investigate the valence distribution of the WO_3 NCs. Fig. 2 shows the XPS survey spectra of WO_3 NCs with corresponding high resolution spectrum of W 4f (W $4f_{5/2}$ and W $4f_{7/2}$) inserted. The three highest peaks in the XPS survey spectra were attributed to W 4f, O 1s and C 1s, respectively. In the high-resolution spectrum of W 4f (inset), the binding energy peaks of W 4f located at 35.8 eV and 37.9 eV were ascribed to the spin-orbit energy splitting of W 4f components (W $4f_{7/2}$ and W $4f_{5/2}$) [30]. The parameters E_pW$4f_{7/2}$ = 35.7 eV and ΔE_p ($4f_{5/2} - 4f_{7/2}$) = 2.1 eV indicated the as-prepared WO_3 NCs were typical W^{6+}-states of oxide [31].

Fig. 3 shows SEM images of WO_3 NCs powders (a) and 0.1 mg mL^{-1} WO_3 NCs dispersion in methanol (b). The particle size of WO_3 NCs powders was about 30 nm and increased to about 60 nm after dispersion in methanol under ultrasonication for 30 min. It was observed that the WO_3 NCs powders could be considerably dispersed into fine and nearly spherical nanoparticles.

Fig. 4 displays PL and UV–vis (inset) spectrum of the WO_3 NCs powders. A strong PL emission peak at 467 nm under the excitation at 350 nm was observed at room temperature. Compared with UV–vis spectrum that shows the maximum adsorption at 350 nm, the PL emission wavelength was about 100 nm red-shifted which could be ascribed to the presence of oxygen vacancies in the WO_3 NCs.

3.2. ECL behavior of $(WO_3)_{NCs}$/Nafion film electrode

It was observed that the ECL intensity of $(WO_3)_{NCs}$/Nafion film electrode in the air-saturated buffer solution was lower than that in the air-free buffer solution. Furthermore, when the air-free buffer solution was then exposed to air, which led to gradually increasing dissolved oxygen, the ECL intensity decreased gradually with increasing exposure time. It indicated that dissolved oxygen would weaken the ECL intensity of $(WO_3)_{NCs}$/Nafion film electrode as the oxygen molecules preferentially adsorbed in the interstitial spaces between neighboring WO_3 NCs drastically lowered the conductivity of interstitial regions [32]. Therefore, the buffer solution was bubbled with highly pure N_2 for 30 min to remove dissolved oxygen in the ECL experiments.

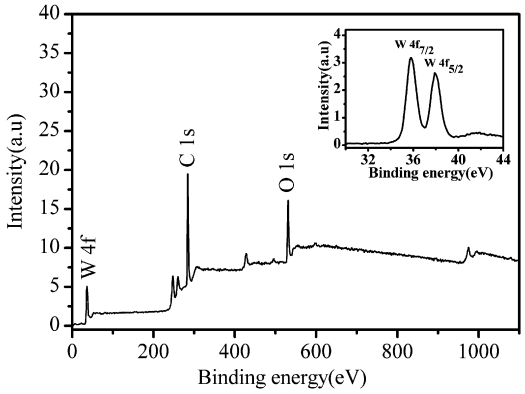

Fig. 2. XPS survey spectra of WO_3 NCs and high resolution spectrum in the (W $4f_{5/2}$ and W $4f_{7/2}$) Binding energy region (inset).

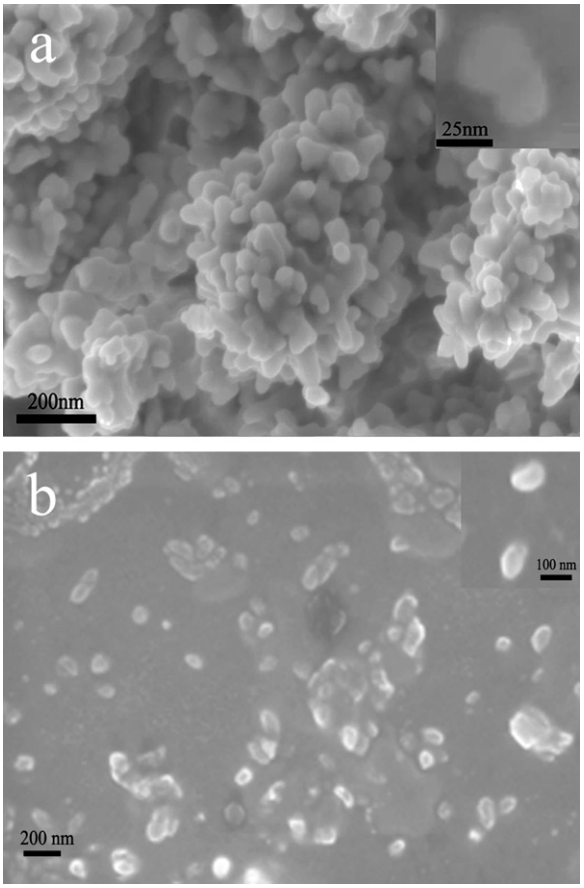

Fig. 3. SEM images of WO_3 NCs powders (a) and 0.1 mg mL^{-1} WO_3 NCs dispersion in methanol under ultrasonication for 30 min (b).

The ECL behavior of $(WO_3)_{NCs}$/Nafion film electrode was greatly affected by the buffer solution with respect to the pH and composition. Fig. 5 shows the pH-dependent ECL intensity of the $(WO_3)_{NCs}$/Nafion film electrode in 0.1 mol L^{-1} HAc–NaAc, NaH_2PO_4–Na_2HPO_4 and NH_3–NH_4Cl buffer solutions, respectively. The cyclic potential was scanned between 0 and 1.4 V with a scan rate of 100 mV s^{-1}. It is clearly shown that the ECL intensity of $(WO_3)_{NCs}$/Nafion film electrode reached the highest value when the pH of solution was around 8. And no obvious ECL signal was observed when the pH of buffer solution was less than 5.5. It could be resulted from the electrochromic reaction of $(WO_3)_{NCs}$/Nafion film under the strong acid condition. Furthermore, the ECL intensity differed when using three different buffer solutions even with

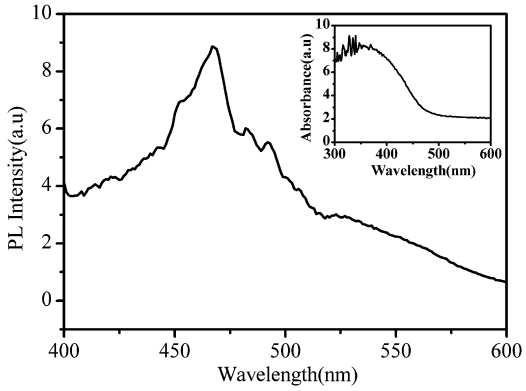

Fig. 4. PL and UV–vis (inset) spectrum of WO_3 NCs powders. Excitation wavelength: 350 nm.

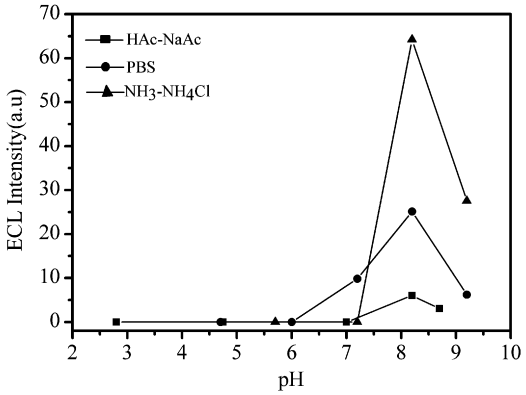

Fig. 5. The ECL of $(WO_3)_{NCs}$/Nafion film electrode in 0.1 mol L^{-1} HAc–NaAc (■), NaH_2PO_4–Na_2HPO_4 (●) and NH_3–NH_4Cl (▲) buffer solution.

the same pH value. The strongest ECL signal was observed when using NH_3–NH_4Cl as the buffer solution. Therefore, 0.1 mol L^{-1} NH_3–NH_4Cl air-free solution at pH 8.2 was used in the latter ECL experiments.Fig. 6 shows the cyclic voltammograms (CVs) (a) and ECL curves (b) of $(WO_3)_{NCs}$/Nafion film electrode with (solid) and without (dash) the presence of 1 mmol L^{-1} TPrA in 0.1 mol L^{-1} NH_3–NH_4Cl solution (pH 8.2). The cyclic potential was scanned forwardly from 0 to 1.4 V and reversely from 1.4 to 0 V with a scan rate of 100 mV s^{-1}. Only a weak ECL peak was observed from Fig. 6b (dash) when the potential was reversely scanned to 1.14 V. No ECL peak was observed on both bare GCE and Nafion modified GCE in the same condition, suggesting that the ECL was due to the existence of WO_3 NCs.

Therefore, it is indicated that WO_3 NCs immobilized on GCE with the help of Nafion could be oxidized or reduced by charge injection during potential cycling and that WO_3 NCs participated in relevant ECL processes. The overall mechanisms are proposed as the following Eqs. (2)–(5). WO_3 NCs could be oxidized to $(WO_3)_{NCs}^{+\bullet}$ when the potential was swept forwardly (Eq. (2)) and then reduced to $(WO_3)_{NCs}^{-\bullet}$ when the potential was swept reversely (Eq. (3)). The oxidized species $(WO_3)_{NCs}^{+\bullet}$ could collide with the reduced species $(WO_3)_{NCs}^{-\bullet}$ in an annihilation process to produce the excited state $(WO_3)_{NCs}^{*}$ which emits photon (Eqs. (4) and (5)).

$$(WO_3)_{NCs} - e \rightarrow (WO_3)_{NCs}^{+\bullet} \quad (2)$$

$$(WO_3)_{NCs} + e \rightarrow (WO_3)_{NCs}^{-\bullet} \quad (3)$$

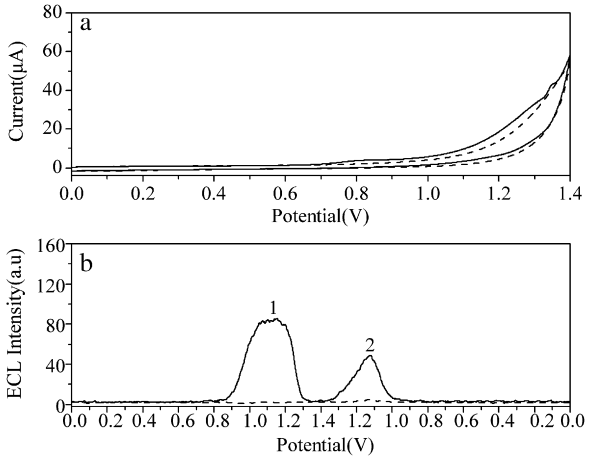

Fig. 6. CVs (A) and ECL (B) curves of $(WO_3)_{NCs}$/Nafion film electrode in 0.1 mol L^{-1} NH_3–NH_4Cl solution (pH 8.2) with (solid) and without (dash) the presence of 1 mmol L^{-1} TPrA.

$$(WO_3)_{NCs}{}^{+\bullet} + (WO_3)_{NCs}{}^{-\bullet} \rightarrow (WO_3)_{NCs}{}^{*} + (WO_3)_{NCs} \quad (4)$$

$$(WO_3)_{NCs}{}^{*} \rightarrow (WO_3)_{NCs} + h\nu \quad (5)$$

However, the ECL signal from the annihilation reaction was weak and unstable, which could be ascribed to the poor stability of electrogenerated species of reaction (4). The poor stability of electrogenerated species, which could be concerned with the aggregation morphology of the WO_3 NCs, was improved by adding the coreactant TPrA to the buffer solution. The corresponding ECL curve is shown in Fig. 6b (solid). In addition to the ECL peak located at 1.14 V (ECL-2), an ECL peak located at 1.13 V (ECL-1) was observed. Moreover, as shown in Fig. 6a, an irreversible peak around 0.8 V was observed in the solid curve but not observed in the dash curve, which implies that ECL-1 involves with the redox of TPrA. Thus, ECL-1 was probably originated from the electron-transfer reaction between the reductant TPrA and the oxidized species $(WO_3)_{NCs}{}^{+\bullet}$. The corresponding ECL processes are proposed as the following Eqs. (6)–(9). WO_3 NCs can be oxidized to $(WO_3)_{NCs}{}^{+\bullet}$ when the potential was swept from 0 to 1.13 V (Eq. (6)). According to previous reports [4], the TPrA can be oxidized to the short-lived $[TPrA^{\bullet}]^{+}$ at 0.8 V and then loses a proton from α-carbon to form the strongly reduced intermediate $TPrA^{\bullet}$ (Eq. (7)). The intermediate $TPrA^{\bullet}$ could react with the oxidized species $(WO_3)_{NCs}{}^{+\bullet}$ to form the excited state $(WO_3)_{NCs}{}^{*}$ which produces light emission (Eqs. (8) and (9)).

$$(WO_3)_{NCs} - e \rightarrow (WO_3)_{NCs}{}^{+\bullet} \quad (6)$$

$$TPrA - e \rightarrow [TPrA^{\bullet}]^{+} \rightarrow TPrA^{\bullet} + H^{+} \quad (7)$$

$$TPrA^{\bullet} + (WO_3)_{NCs}{}^{+\bullet} \rightarrow (WO_3)_{NCs}{}^{*} + TPrA \quad (8)$$

$$(WO_3)_{NCs}{}^{*} \rightarrow (WO_3)_{NCs} + h\nu \quad (9)$$

Apart from processes described above, the WO_3 NCs can continue to be oxidized when the potential was swept from 1.13 to 1.4 V and then reduced when the potential was swept back from 1.4 to 0 V. It is demonstrated by the ECL-2 peak occurred at 1.14 V which was generated from the annihilation reaction between the oxidized species $(WO_3)_{NCs}{}^{+\bullet}$ and the reduced species $(WO_3)_{NCs}{}^{-\bullet}$. The mechanisms of ECL-2 are the same with the above proposed Eqs. (2)–(5). Although ECL-2 showed lower intensity than ECL-1, the intensity of ECL-2 in 0.1 mol L^{-1} NH_3–NH_4Cl solution containing 1 mmol L^{-1} TPrA was enhanced by eight times compared with that in 0.1 mol L^{-1} NH_3–NH_4Cl solution without TPrA.

The proposed mechanisms of ECL-1 and ECL-2 can also be proved by the ECL of WO_3 NCs solution phase. Fig. 7 displays

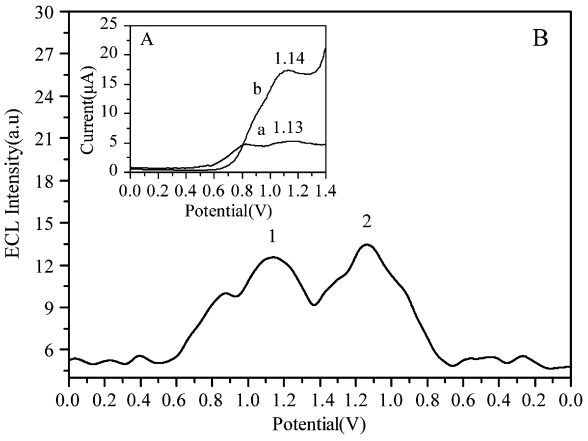

Fig. 7. The DPV curves (A) from 0 to 1.4 V (a) and 1.4 to 0 V (b) and ECL curve (B) of 0.5 mg mL^{-1} WO_3 NCs dispersion in 0.1 mol L^{-1} NH_3–NH_4Cl (pH 8.2) containing 0.25 mmol L^{-1} polyethylene glycol surfactant and 0.01 mol L^{-1} TPrA coreactant.

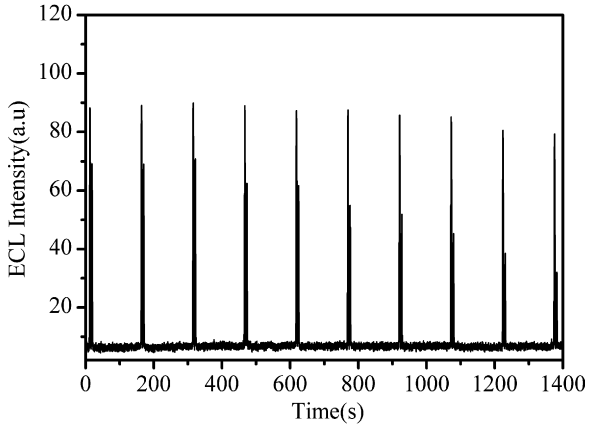

Fig. 8. ECL–time curves of $(WO_3)_{NCs}$/Nafion film electrode in 0.1 mol L^{-1} NH_3–NH_4Cl solution (pH 8.2) containing 1 μmol L^{-1} TPrA under continuous CV scans.

DPV curves (A) and ECL curve (B) of 0.5 mg mL^{-1} WO_3 NCs dispersion in 0.1 mol L^{-1} NH_3–NH_4Cl (pH 8.2) containing 0.25 mmol L^{-1} polyethylene glycol surfactant and 0.01 mol L^{-1} TPrA coreactant. In Fig. 7A, an oxidation peak at 1.13 V (a) and a reduction peak at 1.14 V (b) were ascribed to the oxidation and reduction of WO_3 NCs because these two peaks were not observed in the blank solution without WO_3 NCs. In Fig. 7B, there are two ECL peaks at 1.13 V (ECL-1) and 1.14 V (ECL-2) corresponding to the oxidation (a) and the reduction peak (b) in Fig. 7A. The proposed mechanisms (Eqs. (2)–(9)) are reasonable and consistent with these data.

In order to evaluate the application aspect of this electrode, the stability of the $(WO_3)_{NCs}$/Nafion film electrode was investigated. Fig. 8 displays the ECL emission from the electrode under continuous potential scanning for 10 cycles with a scan rate of 100 mV s^{-1} in 0.1 mol L^{-1} NH_3–NH_4Cl (pH 8.2) containing 1 μmol L^{-1} TPrA. No obvious change of the ECL signal was observed, indicating that the $(WO_3)_{NCs}$/Nafion film electrode exhibits an excellent ECL property and good stability in 0.1 mol L^{-1} NH_3–NH_4Cl (pH 8.2) containing 1 μmol L^{-1} TPrA.

4. Conclusions

In conclusion, the WO_3 NCs and the $(WO_3)_{NCs}$/Nafion film electrode were prepared and the ECL behavior of $(WO_3)_{NCs}$/Nafion film electrode was investigated. The ECL intensity of the $(WO_3)_{NCs}$/Nafion film electrode was significantly influenced by the pH and composition of the buffer solution, and the strongest ECL signal was observed when using the NH_3–NH_4Cl (pH 8.2) as the buffer solution. One ECL peak at 1.14 V and two ECL peaks (1.13 V and 1.14 V) were observed in aqueous solution with the absence and presence of the coreactant TPrA, respectively. The ECL peak at 1.13 V was generated via the electron-transfer process of $(WO_3)_{NCs}{}^{+\bullet}$ and TPrA and the ECL peak at 1.14 V was the product of the annihilation reaction between $(WO_3)_{NCs}{}^{+\bullet}$ and $(WO_3)_{NCs}{}^{-\bullet}$. The $(WO_3)_{NCs}$/Nafion film electrode exhibits excellent ECL property and good stability in 0.1 mol L^{-1} NH_3–NH_4Cl solution containing 1 μmol L^{-1} TPrA (pH 8.2), suggesting that the WO_3 NCs firmly fixed in the Nafion film and not consumed during the potential scan. Therefore, WO_3 NCs could be a good candidate material in fabricating novel ECL sensors for chemical and biochemical analysis.

Acknowledgement

This work is supported by the National Natural Science Foundation of China (no. 20875033).

References

[1] K.A. Fahnrich, M. Pravda, G.G. Guilbault, Talanta 54 (2001) 531–559.
[2] W.-Y. Lee, Mikrochim. Acta 127 (1997) 19–39.
[3] W. Miao, Chem. Rev. 108 (2008) 2506–2553.
[4] M.M. Richter, Chem. Rev. 104 (2004) 3003–3036.
[5] H. Wei, E. Wang, TrAC, Trends Anal. Chem. 27 (2008) 447–459.
[6] W. Guo, J. Yuan, B. Li, Y. Du, E. Ying, E. Wang, Analyst 133 (2008) 1209–1213.
[7] N. Myung, Z. Ding, A.J. Bard, Nano Lett. 2 (2002) 1315–1319.
[8] Y. Bae, N. Myung, A.J. Bard, Nano Lett. 4 (2004) 1153–1161.
[9] Z. Ding, B.M. Quinn, S.K. Haram, L.E. Pell, B.A. Korgel, A.J. Bard, Science 296 (2002) 1293–1297.
[10] N. Myung, X. Lu, K.P. Johnston, A.J. Bard, Nano Lett. 4 (2004) 183–185.
[11] L. Zhang, X. Zou, E. Ying, S. Dong, J. Phys. Chem. C 112 (2008) 4451–4454.
[12] S.K. Poznyak, D.V. Talapin, E.V. Shevchenko, H. Weller, Nano Lett. 4 (2004) 693–698.
[13] G. Wang, Q. Mu, T. Chen, Y. Wang, J. Alloys Compd. 493 (2010) 202–207.
[14] J.-H. Ha, P. Muralidharan, D.K. Kim, J. Alloys Compd. 475 (2009) 446–451.
[15] C.M. Ronconi, C. Ribeiro, L.O.S. Bulhoes, E.C. Pereira, J. Alloys Compd. 466 (2008) 435–438.
[16] M. Salavati-Niasaria, F. Davara, Z. Fereshteh, J. Alloys Compd. 494 (2010) 410–414.
[17] R. Shi, X. Liu, G. Gao, R. Yi, G. Qiu, J. Alloys Compd. 485 (2009) 548–553.
[18] A. Korotcov, H.P. Hsua, Y.S. Huanga, P.C. Liao, D.S. Tsai, K.K. Tiong, J. Alloys Compd. 442 (2007) 310–312.
[19] S. Balaji, Y. Djaoued, A.-S. Albert, R.Z. Ferguson, R. Brüning, Chem. Mater. 21 (2009) 1381–1389.
[20] C. López-Gándara, J.M. Fernández-Sanjuán, F.M. Ramos, A. Cirera, Solid State Ionics 184 (2011) 83–87.
[21] A. Yan, C. Xie, D. Zeng, S. Cai, H. Li, J. Alloys Compd. 495 (2010) 88–92.
[22] Q. Yi, C. Hua, R. Yang, H. Liu, B. Wan, Y. Zhang, J. Alloys Compd. 509 (2011) L255–L261.
[23] S. Salmaoui, F. Sediri, N. Gharbi, C. Perruchot, S. Aeiyach, I.A. Rutkowska, P.J. Kulesza, M. Jouini, Appl. Surf. Sci. 257 (2011) 8223–8229.
[24] C. Sui, J. Gong, T. Cheng, G. Zhou, S. Dong, Appl. Surf. Sci. 257 (2011) 8600–8604.
[25] K.J. Patel, C.J. Panchala, M.S. Desai, P.K. Mehta, Mater. Chem. Phys. 124 (2010) 884–890.
[26] X. Chen, J. Ye, S. Ouyang, T. Kako, Z. Li, Z. Zou, ACS Nano 5 (6) (2011) 4310–4318.
[27] V.S. Vidyarthi, M. Hofmann, A. Savan, K. Sliozberg, D. König, R. Beranek, W. Schuhmann, A. Ludwig, Int. J. Hydrogen Energy 36 (2011) 4724–4731.
[28] M. Feng, A.L. Pan, H.R. Zhang, Z.A. Li, F. Liu, H.W. Liu, D.X. Shi, B.S. Zou, H.J. Gao, Appl. Phys. Lett. 86 (2005) 141901.
[29] S.J Hong, H. Jun, P.H. Borse, J.S. Lee, Int. J. Hydrogen Energy 34 (2009) 3234–3242.
[30] M.W. Xiao, L. Wang, X. Huang, Y. Wu, Z. Dang, J. Alloys Compd. 470 (2009) 486–491.
[31] A.P. Shpak, A.M. Korduban, M.M. Medvedskij, V.O. Kandyba, J. Electron. Spectrosc. Relat. Phenom. 156–158 (2007) 172–175.
[32] L. Ottaviano, E. Maccallini, S. Santicles, Surf. Sci. 492 (2001) L700–L704.